Journal of Nanophotonics

Nanophotonics.SPIEDigitalLibrary.org

Evolution of surface-plasmon-polariton and Dyakonov–Tamm waves with the ambichirality of a partnering dielectric material

Muhammad Faryad
Akhlesh Lakhtakia

SPIE.

Evolution of surface-plasmon-polariton and Dyakonov–Tamm waves with the ambichirality of a partnering dielectric material

Muhammad Faryad* **and Akhlesh Lakhtakia**
Pennsylvania State University, Department of Engineering Science and Mechanics, Nanoengineered Metamaterials Group (NanoMM), University Park, Pennsylvania 16802-6812

Abstract. The planar interface of an isotropic homogeneous metal and an ambichiral dielectric material can guide surface-plasmon-polariton (SPP) waves. The planar interface of an isotropic, homogeneous dielectric material and an ambichiral dielectric material can guide Dyakonov–Tamm waves. In either instance, we found that, as the ambichiral partnering material evolves into a finely chiral material, the solutions of the dispersion equation for surface-wave propagation evince convergence. The convergence is faster for Dyakonov–Tamm waves than for SPP waves. © *2014 Society of Photo-Optical Instrumentation Engineers (SPIE)* [DOI: 10.1117/1.JNP.8.083082]

Keywords: ambichiral material; Dyakonov–Tamm wave; finely chiral material, surface-plasmon-polariton wave.

Paper 14028L received Mar. 9, 2014; revised manuscript received May 21, 2014; accepted for publication May 27, 2014; published online Jun. 25, 2014.

1 Introduction

Anticipating the discovery of cholesteric liquid crystals by about two decades,[1,2] Reusch[3] proposed in 1869 that a periodically nonhomogeneous multilayered material reflects normally incident circularly polarized light of one handedness, but not of the opposite handedness, provided that all layers are made of the same homogeneous, uniaxial dielectric material such that the optic axis in each layer is rotated about the thickness direction with respect to the optic axis in the adjacent layer by a fixed angle. Such a periodically nonhomogeneous dielectric material is nowadays called a Reusch pile.

Extensive theoretical and experimental work by Joly and colleagues[4–7] showed that the circular-polarization-selective reflection of normally incident light by a Reusch pile may occur in several spectral regimes. This selective reflection of circularly polarized light of one handedness, but very little of the other, in a given spectral regime is commonly called the circular Bragg phenomenon.[8,9]

A classification scheme based on the number N of layers in each period of a Reusch pile was developed by Hodgkinson et al.[10] If $N = 2$, the Reusch pile is classified as an equichiral material; if $N > 2$, but not very large, it can be called an ambichiral material; and if $N \to \infty$, it is a finely chiral material. Equichiral materials do not exhibit the circular Bragg phenomenon. Ambichiral materials may exhibit the circular Bragg phenomenon in several spectral regimes, depending on the variations of their constitutive parameters with frequency. A cholesteric liquid crystal[11] can be considered as a finely chiral Reusch pile made of uniaxial dielectric layers.

Reusch piles can also be made of biaxial dielectric material such as columnar thin films (CTFs).[12] A chiral sculptured thin film (STF)[8] can be considered to be a finely chiral Reusch pile comprising biaxial CTFs. Chiral STFs were first fabricated by Young and Kowal[13] in 1959 and were rediscovered in the 1990s.[14] They have been extensively studied since then for optical applications exploiting the circular Bragg phenomenon.[8,9]

*Address all correspondence to: Muhammad Faryad, E-mail: faryad@psu.edu

0091-3286/2014/$25.00 © 2014 SPIE

The effect of the number N of layers in a period on the circular Bragg phenomenon has been studied.[15] Both N and the total number of periods have to be substantially large for the circular Bragg phenomenon to fully develop.[15]

Now, the planar interface of an isotropic homogeneous metal and an ambichiral dielectric material can guide surface-plasmon-polariton (SPP) waves. The planar interface of an isotropic, homogeneous dielectric material and an ambichiral dielectric material can guide Dyakonov–Tamm waves. What is the effect of N on both types of surface waves? The results reported in this communication elucidate the evolution of the solution(s) of the dispersion equation for surface-wave propagation with N.

The plan of this communication is as follows. Section 2 succinctly presents the common formulation of the canonical boundary-value problem for both types of surface waves. Numerical results are presented and discussed in Sec. 3. An $\exp(-i\omega t)$ dependence on time t is implicit, with ω denoting the angular frequency and $i = \sqrt{-1}$. Furthermore, $k_0 = \omega\sqrt{\mu_0\varepsilon_0}$ and $\lambda_0 = 2\pi/k_0$, respectively, represent the free-space wavenumber and free-space wavelength, where μ_0 is the permeability and ε_0 is the permittivity of free space. Vectors are in boldface, dyadics are double-underlined, and the three Cartesian unit vectors are denoted by $\hat{\mathbf{u}}_x$, $\hat{\mathbf{u}}_y$, and $\hat{\mathbf{u}}_z$.

2 Theoretical Preliminaries

The canonical boundary-value problem of surface-wave propagation is depicted schematically in Fig. 1. The half space $z < 0$ is occupied by an isotropic and homogeneous material with relative permittivity ε_s. The half space $z > 0$ is occupied by an ambichiral dielectric material comprising homogeneous layers each of thickness D, the ℓ'th layer occupying the region $(\ell - 1)D < z < \ell D$, $\ell \in [1, \infty)$. The relative permittivity dyadic is given as

$$\underline{\underline{\epsilon}}(z,\omega) = \underline{\underline{S}}_z(h\xi_\ell + h\gamma)\cdot\underline{\underline{S}}_y(\chi)\cdot\underline{\underline{\epsilon}}^{\circ}_{\text{ref}}(\omega)\cdot\underline{\underline{S}}_y^{-1}(\chi)\cdot\underline{\underline{S}}_z^{-1}(h\xi_\ell + h\gamma), \quad (\ell-1)D < z < \ell D, \quad \ell \in [1,\infty), \tag{1}$$

where the reference permittivity dyadic

$$\underline{\underline{\epsilon}}^{\circ}_{\text{ref}}(\omega) = \hat{\mathbf{u}}_z\hat{\mathbf{u}}_z\varepsilon_a(\omega) + \hat{\mathbf{u}}_x\hat{\mathbf{u}}_x\varepsilon_b(\omega) + \hat{\mathbf{u}}_y\hat{\mathbf{u}}_y\varepsilon_c(\omega) \tag{2}$$

contains the eigenvalues $\varepsilon_{a,b,c}(\omega)$ of $\underline{\underline{\epsilon}}(z,\omega)$. The dyadic

$$\underline{\underline{S}}_y(\chi) = (\hat{\mathbf{u}}_x\hat{\mathbf{u}}_x + \hat{\mathbf{u}}_z\hat{\mathbf{u}}_z)\cos\chi + (\hat{\mathbf{u}}_z\hat{\mathbf{u}}_x - \hat{\mathbf{u}}_x\hat{\mathbf{u}}_z)\sin\chi + \hat{\mathbf{u}}_y\hat{\mathbf{u}}_y \tag{3}$$

depends on the tilt angle $\chi \in [0\ \text{deg}, 90\ \text{deg}]$ with respect to the xy plane, the dyadic

$$\underline{\underline{S}}_z(\xi) = (\hat{\mathbf{u}}_x\hat{\mathbf{u}}_x + \hat{\mathbf{u}}_y\hat{\mathbf{u}}_y)\cos\xi + (\hat{\mathbf{u}}_y\hat{\mathbf{u}}_x - \hat{\mathbf{u}}_x\hat{\mathbf{u}}_y)\sin\xi + \hat{\mathbf{u}}_z\hat{\mathbf{u}}_z \tag{4}$$

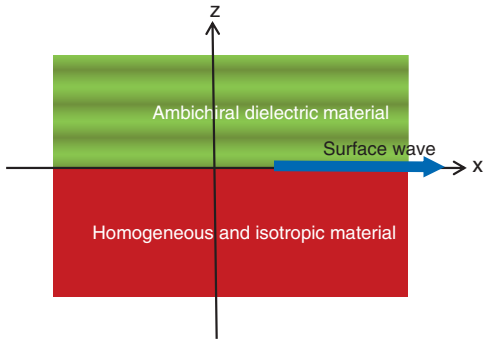

Fig. 1 Schematic of the canonical boundary-value problem.

represents a rotation about the z axis by an angle ξ, $\xi_\ell = (\ell - 1)\pi/N$ with $N \geq 1$ being the number of layers in each period $2\Omega = ND$, Ω is the half period, right-handed rotation is represented by $h = 1$ and left-handed rotation by $h = -1$, and γ is an angular offset with respect to the x axis.

In the region $z < 0$, the electric field phasor may be written as[16–18]

$$\mathbf{E}(x,z) = \left[a_1 \hat{\mathbf{u}}_y + a_2 \left(\frac{\alpha_s \hat{\mathbf{u}}_x + q \hat{\mathbf{u}}_z}{k_0 n_s} \right) \right] \exp[i(qx - \alpha_s z)], \qquad z < 0, \tag{5}$$

where $q^2 + \alpha_s^2 = k_0^2 \varepsilon_s$, $n_s = \sqrt{\varepsilon_s}$, q is the complex-valued wavenumber of the surface wave, $\mathrm{Im}(\alpha_s) > 0$ for attenuation as $z \to -\infty$, and a_1 and a_2 are unknown scalars with the same units as the electric field.

For field representation in the region $z > 0$, let us write[18]

$$\mathbf{E}(x,z) = \mathbf{e}(z) \exp(iqx), \qquad \mathbf{H}(x,z) = \mathbf{h}(z) \exp(iqx). \tag{6}$$

The Cartesian components of the electric and magnetic field phasors tangential to the xy plane are used to form the column vector

$$[\mathbf{f}(z)] = \begin{bmatrix} e_x(z) \\ e_y(z) \\ h_x(z) \\ h_y(z) \end{bmatrix} \tag{7}$$

which satisfies the matrix differential equation

$$\frac{\mathrm{d}}{\mathrm{d}z} [\mathbf{f}(z)] = i [\underline{\underline{P}}(z)] \cdot [\mathbf{f}(z)], \qquad z > 0, \tag{8}$$

where the 4×4 matrix $[\underline{\underline{P}}(z)]$ depends not only on $\underline{\underline{\varepsilon}}(z, \omega)$ but also on q.

The piecewise-uniform approximation technique[8] can be used to determine the matrix $[\underline{\underline{\tilde{Q}}}]$ that appears in the relation

$$[\mathbf{f}(2\Omega)] = \exp\{i 2\Omega [\underline{\underline{\tilde{Q}}}]\} \cdot [\mathbf{f}(0+)] \tag{9}$$

for specific values of q. Let $[\mathbf{t}]^{(n)}$, $n \in [1,4]$, be the eigenvector corresponding to the n'th eigenvalue α_n of $[\underline{\underline{\tilde{Q}}}]$. After ensuring that $\mathrm{Im}(\alpha_{1,2}) > 0$, we set

$$[\mathbf{f}(0+)] = \left[[\mathbf{t}]^{(1)} \quad [\mathbf{t}]^{(2)} \right] \cdot \begin{bmatrix} b_1 \\ b_2 \end{bmatrix} \tag{10}$$

for surface-wave propagation, where b_1 and b_2 are unknown dimensionless scalars; the other two eigenvalues of $[\underline{\underline{\tilde{Q}}}]$ pertain to waves that amplify as $z \to \infty$ and cannot therefore contribute to the surface wave. At the same time, $[\mathbf{f}(0-)]$ can be obtained from Eq. (5) and the corresponding magnetic field phasor $\mathbf{H} = -i \nabla \times \mathbf{E} / \omega \mu_0$.

Enforcement of the usual boundary conditions across the plane $z = 0$ requires that $[\mathbf{f}(0-)] = [\mathbf{f}(0+)]$, which may be rearranged as the matrix equation

$$[\underline{\underline{Y}}] \cdot \begin{bmatrix} a_1 \\ a_2 \\ b_1 \\ b_2 \end{bmatrix} = \begin{bmatrix} 0 \\ 0 \\ 0 \\ 0 \end{bmatrix}, \tag{11}$$

leading to the dispersion equation

$$\det[\underline{\underline{Y}}(q)] = 0. \tag{12}$$

3 Numerical Results and Discussion

The dispersion equation (12) was solved using the Newton–Raphson method,[19] with λ_0 fixed at 633 nm. For all numerical results presented here, the ambichiral dielectric material was taken to comprise CTFs made by directing a collimated evaporant flux of patinal titanium oxide in a low-pressure chamber at a fixed angle $\chi_v \in (0 \text{ deg}, 90 \text{ deg}]$ with respect to a planar substrate.[20] For the chosen CTF,

$$\begin{cases} \varepsilon_a = [1.0443 + 2.7394(2\chi_v/\pi) - 1.3697(2\chi_v/\pi)^2]^2 \\ \varepsilon_b = [1.6765 + 1.5649(2\chi_v/\pi) - 0.7825(2\chi_v/\pi)^2]^2 \\ \varepsilon_c = [1.3586 + 2.1109(2\chi_v/\pi) - 1.0554(2\chi_v/\pi)^2]^2 \\ \chi = \tan^{-1}(2.8818 \tan\chi_v) \end{cases} \tag{13}$$

according to Hazel and co-workers.[20] We fixed $\Omega = 200$ nm, while varying $N \in [1, 15]$ (so that $D = 2\Omega/N$ was simultaneously varied) and $\gamma \in \{0 \text{ deg}, 45 \text{ deg}, 90 \text{ deg}\}$. Furthermore, $\chi_v = 20$ deg was fixed so that $\varepsilon_a = 2.5135$, $\varepsilon_b = 3.9426$, and $\varepsilon_c = 3.1528$.

3.1 *Surface-Plasmon-Polariton Waves*

Let the isotropic homogeneous partnering material be thin-film aluminum with $\varepsilon_s = -14.65 + i5.85$ (Ref. 21) at $\lambda_0 = 633$ nm. Then, all solutions q of the dispersion equation (12) represent SPP waves.[16,18] These solutions are complex valued because ε_s is complex valued.

Only one solution of the dispersion equation exists for any $\gamma \in [0 \text{ deg}, 90 \text{ deg}]$ when the anisotropic partnering material is homogeneous (i.e., $N = 1$).[22] However, when that partnering material is periodically nonhomogeneous (i.e., $N > 1$), the solutions can be organized into two branches for $\gamma = 0$ deg and 45 deg but only one for $\gamma = 90$ deg, as shown in Fig. 2. Convergence on either branch is monotonic for $N > 2$.

The most notable feature of the solutions presented in Fig. 2 is their evolution and convergence as N increases. Although not shown in this figure, both the real and imaginary parts of q on the first branch in Fig. 2 lie within 0.1% of the corresponding solutions for the metal/chiral-STF interface[16] when $N \geq 18$, and on the second branch in that figure lie within 0.1% when $N \geq 55$. Also, $\mathrm{Re}(q)$ converges faster with respect to N than $\mathrm{Im}(q)$ does.

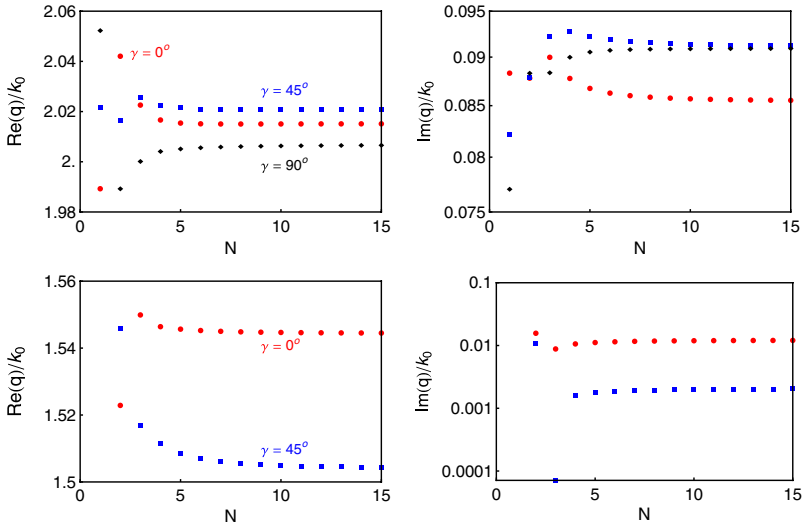

Fig. 2 Real and imaginary parts of the solutions q of Eq. (12) as functions of $N \in [1, 15]$ and $\gamma \in \{0 \text{ deg}, 45 \text{ deg}, 90 \text{ deg}\}$ for SPP waves guided by the planar interface of aluminum ($\varepsilon_s = -14.65 + i5.85$) and an ambichiral dielectric material characterized by Eq. (13) with $\chi_v = 20$ deg, when $\lambda_0 = 633$ nm and $\Omega = 200$ nm. Top panels: First branch of solutions. Bottom panels: Second branch of solutions.

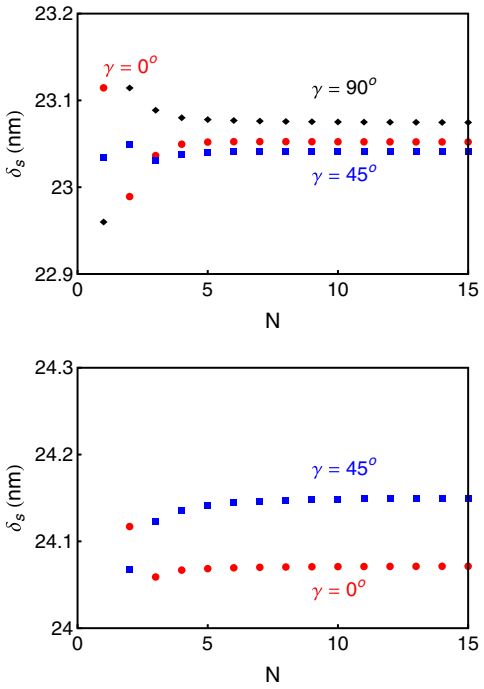

Fig. 3 The penetration depth δ_s of SPP waves into aluminum for the (top) first and (bottom) second branches of solutions provided in Fig. 2.

In order to delineate the effect of N on the localization of SPP waves to the interface $z = 0$, the penetration depth $\delta_s = 1/\mathrm{Im}(\alpha_s)$ into aluminum is presented in Fig. 3 in relation to N for all solutions of Eq. (12). The penetration depth converges to $\simeq$23 nm for the first branch and to $\simeq$24 nm for the second branch as N increases.

Since the ambichiral material is periodically nonhomogeneous and anisotropic, two decay constants $\beta_{1,2} = \exp[-2\Omega\mathrm{Im}(\alpha_{1,2})] \in (0, 1)$ are defined[18] to quantify localization in the anisotropic partnering material. The smaller that $\min\{\beta_1, \beta_2\}$ is, the higher is that localization of the SPP wave to the interface. The decay constants for all SPP waves found are presented in Fig. 4.

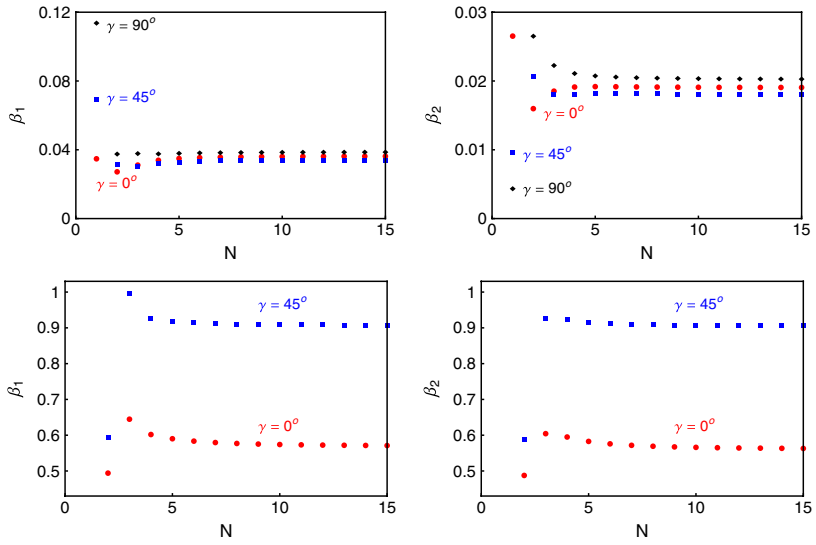

Fig. 4 The decay constants $\beta_{1,2}$ of SPP waves for the (top) first and (bottom) second branches of solutions provided in Fig. 2.

The SPP waves on the first branch are highly localized to the interface within the ambichiral material as both decay constants converge to values <0.05 with increasing N. The SPP waves on the second branch are loosely bound to the interface, and the degree of localization strongly depends on the direction of propagation. Both decay constants converge to $\simeq 0.6$ for $\gamma = 0$ deg, but both converge to $\simeq 0.9$ for $\gamma = 45$ deg. Furthermore, data for $N > 15$ (not shown) indicated that δ_s, β_1, and β_2 converge to within 0.1% of their respective values when $N \geq 29$ on the first branch and $N \geq 30$ on the second branch.

3.2 *Dyakonov–Tamm Waves*

Next, let the isotropic homogeneous partnering material be magnesium fluoride—a dielectric material with $\varepsilon_s = 1.896$ at $\lambda_0 = 633$ nm—instead of a metal. Every solution of the dispersion equation (12) represents a Dyakonov–Tamm wave[17]—named thus because this wave has the attributes of both the Dyakonov wave[23,24] and the Tamm wave[18,25]—since both partnering materials are dielectric materials and one of the two is anisotropic and periodically nonhomogeneous normal to the waveguiding interface for $N \geq 2$.[17,18]

For every $\gamma \in \{0 \text{ deg}, 45 \text{ deg}, 90 \text{ deg}\}$, only one solution of Eq. (12) was found. Dissipation being absent in both partnering materials, q is real valued. The dependence of q on N is shown in Fig. 5. Also provided in the same figure are δ_s and $\beta_{1,2}$ in relation to N.

For $N = 1$, the anisotropic partner is homogeneous and the solution q for $\gamma = 0$ deg represents a Dyakonov wave;[23,24] no solution was found for $\gamma \in \{45 \text{ deg}, 90 \text{ deg}\}$. For $N > 1$, only one solution was found regardless of the value of γ, and that solution represents a Dyakonov–Tamm wave. Figure 5 indicates the typical difference between Dyakonov and Dyakonov–Tamm waves:[17] The range of γ is much larger for surface waves of the latter type than for the surface waves of the former type.

Just like the solutions presented in Fig. 2 for SPP waves, those presented in Fig. 5 for Dyakonov–Tamm waves also evolve as N increases. Specifically, the solutions in Fig. 5 converge monotonically to within 0.1% of the corresponding solution for the isotropic-dielectric/chiral-STF interface[17] when $N \geq 9$.

Figure 5 shows that the penetration depth of the Dyakonov–Tamm wave into the homogeneous partnering material depends upon γ and, hence, the direction of propagation,

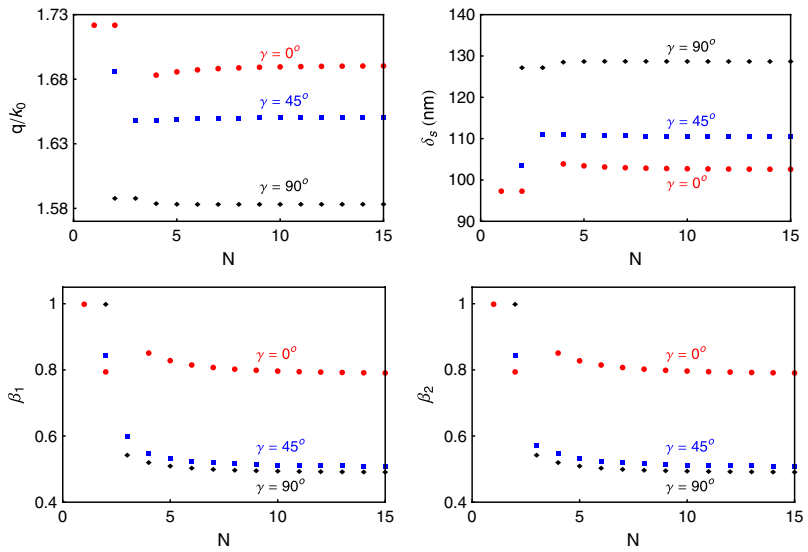

Fig. 5 Solution q, penetration depth δ_s into magnesium fluoride ($\varepsilon_s = 1.896$), and the decay constants $\beta_{1,2}$ in the ambichiral dielectric material characterized by Eqs. (13) with $\chi_v = 20$ deg, as functions of $N \in [1, 15]$ and $\gamma \in \{0 \text{ deg}, 45 \text{ deg}, 90 \text{ deg}\}$, for Dyakonov–Tamm waves guided by the interface of magnesium fluoride and the ambichiral dielectric material, when $\lambda_0 = 633$ nm and $\Omega = 200$ nm.

but is about four times greater than for SPP waves. The plots of the decay constants show that the degree of localization of the Dyakonov–Tamm wave in the ambichiral material increases as γ increases. The values of $\beta_{1,2}$ converge to $\simeq 0.8$ for $\gamma = 0$ deg and to $\simeq 0.5$ for $\gamma = 45$ deg and 90 deg. Furthermore, δ_s, β_1, and β_2 converge to within 0.1% when $N \geq 32$.

3.3 *Sufficient Value of N*

In order to fabricate a structurally chiral material with continuous variation of $\underline{\underline{\varepsilon}}(z,\omega)$ with z as an ambichiral material, a sufficient value of N must be chosen based upon the tolerances in the values of the wavenumber q, penetration depth δ_s, and the smaller decay constant $\min\{\beta_1, \beta_2\}$. If all tolerances are chosen to be 0.1%, as in the previous subsections, $N = 55$ is sufficient for the SPP wave, and $N = 32$ for the Dyakonov–Tamm wave. However, if all tolerances are chosen to be 1%, $N = 19$ suffices for the SPP wave and $N = 11$ for the Dyakonov–Tamm wave.

Let us note that the thickness D of each CTF in the ambichiral material is $2\Omega/N \simeq 21$ nm for $N = 19$ and $\simeq 36$ nm for $N = 11$. If the thickness of each CTF either equals or is less than one-tenth of the smallest wavelength inside the ambichiral material, then each CTF is electrically thin.[26] For the chosen parameters, one-tenth of the smallest wavelength inside the ambichiral material is $\lambda_0/(10\sqrt{\varepsilon_b}) \simeq 32$ nm since $\varepsilon_b > \varepsilon_c > \varepsilon_a > 1$. Therefore, if $D \leq \lambda_0/(10\sqrt{\max\{\varepsilon_a, \varepsilon_b, \varepsilon_c\}})$, the ambichiral material has a sufficiently smooth variation of $\underline{\underline{\varepsilon}}(z,\omega)$ with z and all important quantities characterizing a surface wave will converge to within $\sim 1\%$.

4 Concluding Remarks

The canonical boundary-value problem of surface-wave propagation guided by the planar interface of an isotropic homogeneous material and an ambichiral material was set up and solved. Both SPP and Dyakonov–Tamm waves were investigated. As the number N of layers per period in the ambichiral partnering material was increased, the solutions of the dispersion equation for surface-wave propagation were found to converge to those for the ambichiral material replaced by the corresponding finely chiral material. The convergence is faster when the homogeneous partnering material is dielectric than when it is metallic. The real part of the wavenumber q of an SPP wave converges faster than the imaginary part with respect to N. The real and imaginary parts of the surface wavenumber, the penetration depth into the isotropic partner, and the decay constants in the ambichiral dielectric material converge to within $\sim 1\%$ if the layers in the ambichiral material are electrically thin.

Acknowledgments

MF and AL are grateful for partial support from Grant No. DMR-1125591 of the US National Science Foundation. AL is also grateful to the Charles Godfrey Binder Endowment at the Pennsylvania State University for partial support of this work.

References

1. F. Reinitzer, "Beiträge zur Kenntiss des Cholesterins," *Monat. Chem. (Wien)* **9**(1), 421–441 (1888).
2. T. J. Sluckin, D. A. Dunmur, and H. Stegemeyer, *Crystals That Flow: Classic Papers From the History of Liquid Crystals*, Taylor & Francis, London (2004).
3. E. Reusch, "Untersuchung über Glimmercombinationen," *Ann. Phys. Chem. Lpz.* **138**(12), 628–638 (1869).
4. G. Joly and J. Billard, "Quelques champs électromagnétiques dans les piles de Reusch I.—Les vibrations propres d'une pile de deux lames a biréfringence rectiligne ne sont pas orthogonales," *J. Opt. (Paris)* **12**(5), 323–329 (1981).

5. G. Joly and J. Billard, "Quelques champs électromagnétiques dans les piles de Reusch II. Piles éclairées sous l'incidence normale par des ondes monochromatiques planes et uniformes," *J. Opt. (Paris)* **13**(4), 227–238 (1982).
6. G. Joly and N. Isaert, "Quelques champs électromagnétiques dans les piles de Reusch III. Biréfringence elliptique des vibrations itératives; activité optique de piles hélicoïdales d'extension finie," *J. Opt. (Paris)* **16**(5), 203–213 (1985).
7. G. Joly and N. Isaert, "Quelques champs électromagnétiques dans les piles de Reusch IV—Domaines multiples de réflexion sélective," *J. Opt. (Paris)* **17**(5), 211–221 (1986).
8. A. Lakhtakia and R. Messier, *Sculptured Thin Films: Nanoengineered Morphology and Optics*, SPIE Press, Bellingham, Washington (2005).
9. M. Faryad and A. Lakhtakia, "The circular Bragg phenomenon," *Adv. Opt. Photon.* **6**(2), 225–292 (2014).
10. I. J. Hodgkinson et al., "Ambichiral, equichiral and finely chiral layered structures," *Opt. Commun.* **239**(4–6), 353–358 (2004).
11. P. G. de Gennes and J. A. Prost, *The Physics of Liquid Crystals*, 2nd ed., Clarendon, Oxford (1993).
12. I. J. Hodgkinson and Q.-h. Wu, *Birefringent Thin Films and Polarizing Elements*, World Scientific, Singapore (1997).
13. N. O. Young and J. Kowal, "Optically active fluorite films," *Nature* **183**(4654), 104–105 (1959).
14. K. Robbie, M. J. Brett, and A. Lakhtakia, "First thin film realization of a helicoidal bianisotropic medium," *J. Vac. Sci. Technol. A* **13**(6), 2991–2993 (1995).
15. I. Abdulhalim, "Effect of the number of sublayers on axial optics of anisotropic helical structures," *Appl. Opt.* **47**(16), 3002–3008 (2008).
16. J. A. Polo Jr. and A. Lakhtakia, "On the surface plasmon polariton wave at the planar interface of a metal and a chiral sculptured thin film," *Proc. R. Soc. Lond. A* **465**(2101), 87–107 (2009).
17. A. Lakhtakia and J. A. Polo, Jr., "Dyakonov–Tamm wave at the planar interface of a chiral sculptured thin film and an isotropic dielectric material," *J. Eur. Opt. Soc.–Rapid Publ.* **2**(1), 07021 (2007).
18. J. A. Polo Jr., T. G. Mackay, and A. Lakhtakia, *Electromagnetic Surface Waves: A Modern Perspective*, Elsevier, Waltham, MA (2013).
19. Y. Jaluria, *Computer Methods for Engineering*, Taylor & Francis, Washington, DC (1996).
20. I. J. Hodgkinson, Q. h. Wu, and J. Hazel, "Empirical equations for the principal refractive indices and column angle of obliquely-deposited films of tantalum oxide, titanium oxide and zirconium oxide," *Appl. Opt.* **37**(13), 2653–2659 (1998).
21. A. Lakhtakia, Y.-J. Jen, and C.-F. Lin, "Multiple trains of same-color surface plasmon-polaritons guided by the planar interface of a metal and a sculptured nematic thin film. Part III: Experimental evidence," *J. Nanophoton.* **3**(1), 033506 (2009).
22. J. A. Polo Jr. and A. Lakhtakia, "Morphological effects on surface-plasmon-polariton waves at the planar interface of a metal and a columnar thin film," *Opt. Commun.* **281**(21), 5453–5457 (2008).
23. M. I. Dyakonov, "New type of electromagnetic wave propagating at an interface," *Sov. Phys. JETP* **67**(4), 714–716 (1988).
24. O. Takayama et al., "Dyakonov surface waves: a review," *Electromagnetics* **28**(3), 126–174 (2008).
25. P. Yeh, A. Yariv, and C.-S. Hong, "Electromagnetic propagation in periodic stratified media. I. General theory," *J. Opt. Soc. Am.* **67**(4), 423–438 (1977).
26. P. S. Reese and A. Lakhtakia, "Low-frequency electromagnetic properties of an alternating stack of thin uniaxial dielectric laminae and uniaxial magnetic laminae," *Z. Naturforsch. A* **46**(5), 384–388 (1991).

Muhammad Faryad received his MSc and MPhil degrees in electronics from Quaid-i-Azam University in 2006 and 2008, respectively, and his PhD (2012) degree in engineering science and mechanics from the Pennsylvania State University, where he is presently a postdoctoral research scholar. His research interests include modeling of thin-film solar cells, electromagnetic surface waves, chemical sensing, circular Bragg phenomenon, and sculptured thin films.

Akhlesh Lakhtakia is the Charles Godfrey Binder (Endowed) professor of Engineering Science and Mechanics at the Pennsylvania State University. He is a fellow of SPIE, Optical Society of America, American Association for the Advancement of Science, American Physical Society, and Institute of Physics (United Kingdom). He was the sole recipient of the 2010 SPIE Technical Achievement Award. His current research interests include nanophotonics, surface multiplasmonics, complex materials including mimumes and sculptured thin films, bone refacing, bioreplication, and forensic science.